# The Formation and Evolution of Virgo Cluster Galaxies – I. Broadband Optical & Infrared Colours

Joel C. Roediger and Stéphane Courteau

Department of Physics, Engineering Physics & Astronomy, Queen's University, Kingston, Ontario, Canada

#### Michael McDonald

Dept. of Astronomy, University of Maryland, College Park, MD

and

#### Lauren A. MacArthur

Herzberg Institute of Astrophysics, National Research Council of Canada, 5071 West Saanich Road, Victoria, BC, Canada

## **ABSTRACT**

We use a combination of deep optical (gri) and near-infrared (H) photometry to study the radially-resolved colours of a broad sample of Virgo cluster galaxies. For most galaxy types, we find that the median g-H colour gradient is either flat (gas-poor giants and gas-rich dwarfs) or negative (i.e., colours become bluer with increasing radius; gas-poor dwarfs, spirals, and gas-poor peculiars). Also, later-type galaxies typically exhibit more negative gradients than early-types. Given the lack of a correlation between the central colours and axis ratios of Virgo spiral galaxies, we argue that dust likely plays a small role, if at all, in setting those colour gradients. We search for possible correlations between galaxy colour and photometric structure or environment and find that the Virgo galaxy colours become redder with increasing concentration, luminosity and surface brightness, while no dependence with cluster-centric radius or local galaxy density is detected (over a range of  $\sim$ 2 Mpc and  $\sim$ 3 – 16 Mpc–2, respectively). However, the colours of gas-rich Virgo galaxies do correlate with neutral gas deficiency, such that these galaxies become redder with higher deficiencies.

Comparisons with stellar population models suggest that these colour gradients arise principally from variations in stellar metallicity within these galaxies, while age variations only make a significant contribution to the colour gradients of Virgo irregulars. This paper serves as an introduction to a detailed stellar population analysis of Virgo cluster galaxies by the same authors (Roediger et al 2011b).

```
Subject headings: galaxies: clusters: individual (Virgo) — galaxies: dwarf — galaxies: elliptical — galaxies: lenticular — galaxies: evolution — galaxies: formation — galaxies: irregular — galaxies: peculiar — galaxies: spiral — galaxies: stellar content — galaxies: structure
```

#### 1. INTRODUCTION

The broadband colours of galaxies reveal information about the ages and metallicities of their stellar populations (as well as their dust content). Galaxy colours thus provide a fundamental means for the investigation of both their star formation histories and chemical evolution, a fact which is reflected by the rich history of this field (e.g., Vader et al. 1988; Peletier et al. 1990; Goudfrooij et al. 1994; de Jong 1996; Bell & de Jong 2000; MacArthur et al. 2004; van Zee et al. 2004; Taylor et al. 2005) since the pioneering works of Searle et al. (1973) and Tinsley & Gunn (1976).

The alternative to colour-based analyses of galaxies' stellar populations involves a spectroscopic approach, either through the measurement of absorption line strengths (e.g., Faber 1973; Terlevich et al. 1981; Burstein et al. 1984; Worthey et al. 1992; Kobayashi & Arimoto 1999; Trager et al. 2000; Gallazzi et al. 2005; Peletier et al. 2007) or the synthesis of entire spectra (e.g., MacArthur et al. 2009). The benefits of the spectroscopic approach include a cleaner separation of the correlated age and metallicity effects (Worthey 1994) and, in the case of the Lick indices, a global insensitivity to dust reddening (MacArthur 2005). Spectroscopic stellar population studies demand some appreciable trade-offs compared to colour-based analyses however, such as smaller sample sizes and shallower depths. Colours then offer the most efficient means to simultaneously obtain deep radially-resolved and representative stellar population information for large numbers of galaxies.

Through comparison with stellar population models, galaxies' colour gradients may be decomposed into corresponding gradients of age and metallicity. The latter data provide a record of the build-up of galaxies' stellar contents and so are naturally of great value to galaxy formation and evolution models. In modelling galaxy colours, a wide and well-sampled wavelength baseline (i.e., ultraviolet, UV, to infrared; Gavazzi et al. 2002) is certainly desirable, not only to better constrain the fits, but also to overcome the age-metallicity degeneracy which plagues optical stellar popula-

tion studies (Worthey 1994). Although the availability of space-based imaging (i.e., GALEX) has provided a much desired wavelength expansion of colour-based studies (e.g., Boselli et al. 2008), the use of optical and near-infrared (NIR) data alone already goes a long way towards overcoming the above degeneracy (Cardiel et al. 2003).

Radially-resolved studies of galaxy colours abound in the literature. For giant gas-poor galaxies (E/S0), the consensus seems to be that they possess negative colour gradients (Peletier & Valentijn 1989; Peletier et al. 1990; Goudfrooij et al. 1994; Silva & Elston 1994; Michard 1999; Wu et al. 2005; James et al. 2006; La Barbera & de Carvalho 2009; Gonzalez-Perez et al. 2011; La Barbera et al. 2010), the cause of which is popularly attributed to an outward decrease in stellar metallicity (Vader et al. 1988; Franx et al. 1989; Tamura et al. 2000; Tamura & Ohta 2000, 2003; La Barbera et al. 2004). Positive UV and optical colour gradients found in both local and high-z E/S0's (Michard 2000; Moth & Elston 2002; Menanteau et al. 2004; Ferreras et al. 2009; Suh et al. 2010), however, imply that centralized star formation has recently occurred, thereby arguing for at least a partial age gradient contribution.

Discerning the nature of spiral galaxies' colour gradients is inherently complicated due to the presence of dust, gas, and multiple stellar populations within them (Kim & Ann 1990; Gadotti & dos Anjos 2001; Koo et al. 2005; Taylor et al. 2005; Ganda et al. 2009; Liu et al. 2009). This complexity may be lifted though by distinguishing between early- and late-type spirals, wherein the former have flat or negative colour gradients (Terndrup et al. 1994; de Jong 1996; Peletier & Balcells 1996; Moriondo et al. 2001; Ganda et al. 2009) while the latter are described by positive colour gradients, but with a wide dispersion (Kim & Ann 1990; Taylor et al. 2005; Tamm & Tenjes 2006; Liu et al. 2009). Given such a variety, it is not surprising that spiral galaxies' colour gradients have often been ascribed to both age and metallicity effects, with dust making a second-order or altogether negligible contribution (de Jong 1996; Peletier & Balcells 1996; Gadotti & dos Anjos 2001; MacArthur et al. 2004, ; however, see Ganda et al. 2009).

Lastly, the colour gradients amongst the remaining galaxy types are more uniform than those found in spirals. That is, both peculiar and (gas-rich and gas-poor) dwarf galaxies are typically described by positive colour gradients (Vader et al. 1988; Jerjen et al. 2000; Kim & Ann 1990; James 1994; Papaderos et al. 1996; Tully et al. 1996; Barazza et al. 2003; van Zee et al. 2004; Taylor et al. 2005). Since the notion of such galaxies having a higher metallicity in their outskirts (where the potential is weaker) seems highly counter-intuitive, these colour gradients have commonly been attributed to underlying positive age gradients within them<sup>1</sup> (e.g., Vader et al. 1988). Negative metallicity gradients, on the other hand, may very well contribute to the flat and negative

<sup>&</sup>lt;sup>1</sup>The effects of dust and recent star formation may, however, also contribute to the positive colour gradients in gas-poor dwarfs.

colour gradients that have been observed within a minority of dwarf galaxies (Patterson & Thuan 1996; Parodi et al. 2002; Barazza et al. 2003; van Zee et al. 2004).

Aside from the typical colour gradient for each principal morphological type, the structural or environmental parameters which correlate with galaxies' colours and colour gradients are also of interest to understanding galaxy formation. The most prevalent of such correlations for all galaxy types are those against luminosity (Balcells & Peletier 1994; Jansen et al. 2000; Tamura & Ohta 2003; Muñoz-Mateos et al. 2007; Liu et al. 2009; Tortora et al. 2010), mass (Vader et al. 1988; MacArthur et al. 2004; West et al. 2009; La Barbera et al. 2010; Suh et al. 2010), colour (Tully et al. 1996; Pierini 2002; Gadotti & dos Anjos 2001; Ferreras et al. 2005, 2009), and size (Bergvall et al. 1999; Parodi et al. 2002; Tamura & Ohta 2003; Muñoz-Mateos et al. 2007; Liu et al. 2009; Tortora et al. 2010), in the sense that more luminous, more massive, redder, and larger galaxies have reddest colours and flattest colour gradients. In addition, spiral galaxies have bluer colours and steeper colour gradients for lower surface brightnesses (de Jong 1996; Liu et al. 2009) and larger HI contents (West et al. 2009). Less uniformity has been found amongst galaxy types with respect to the environmental dependence of their colour information, however. While the colour gradients of gas-poor giants flatten (Ko & Im 2005; La Barbera et al. 2005) and the colours of gas-rich dwarfs redden (Gallagher & Hunter 1986; Parodi et al. 2002) towards high densities, no corresponding trends have been found amongst spiral galaxies (Koo et al. 2005; Muñoz-Mateos et al. 2007).

Despite the seemingly coherent picture presented above based upon piecemeal information, a homogeneous analysis of galaxy colours and colour gradients across all galaxy types which incorporates NIR data would enable a valuable confirmation of that picture. Thus, we present here the resolved optical and optical-NIR colours of a sample of Virgo cluster galaxies that spans the full range in galaxy morphology. This paper is organized as follows. In §2 we discuss the salient aspects and organisation of our photometric database. Broadband colour gradients, as well as morphological, structural, and environmental trends with galaxy colours are shown and discussed in the context of previous work in §3. The interpretation of our results in terms of the stellar populations of Virgo cluster galaxies, however, is addressed in a companion paper (Roediger et al. 2011b; hereafter, Paper II). Conclusions are provided in §4. Throughout this paper, we assume a distance of 16.5 Mpc to all Virgo cluster galaxies (Mei et al. 2007) and refer to both S0 and S0/a galaxy types simply as "S0".

## 2. DATA

A systematic study of the colours and stellar populations within galaxies of all types demands as complete a volume-limited sample as possible. Given that the Virgo cluster is the closest large concentration of galaxies whose members span the full range of galaxian parameter space, we use

for our study the radially-resolved *griH* photometric database derived from the imaging survey of Virgo galaxies of McDonald et al. (2011, hereafter M11). Only those aspects of M11 which are relevant to our study are discussed below; further details can be found in M11.

The M11 sample includes 285 galaxies selected from the Virgo Cluster Catalog (Binggeli et al. 1985, hereafter VCC); it is nearly complete down to  $B \sim 16$  ( $M_B \sim -15$ ). For each galaxy, Sloan Digital Sky Survey (Adelman-McCarthy et al. 2007, 2008, hereafter SDSS) gri- and separate H-band imaging is available. The spatial distribution and completeness of this sample are shown in Figures 1 & 2 of M11. The M11 sample extends out to the  $6^{\circ}$  radius of the Virgo cluster (McLaughlin 1999), such that the sample spans a wide range in environmental conditions (i.e., galaxy densities  $\Sigma \sim 3-16$  Mpc<sup>-2</sup> and gas deficiencies  $Def_{HI} \sim -0.4-2.3$  dex; see §2.3. As seen in M11, a natural bias for gas-poor galaxies exists in the sample given the morphology-density relation (Dressler 1980). Nevertheless, the M11 sample contains 86 gas-rich galaxies (56 giants and 30 dwarfs; see Table 1), thereby allowing for meaningful comparisons of the colours, and thus stellar populations, between major Virgo galaxy types.

# 2.1. Photometry

Radially-resolved optical (ugriz) photometry for the M11 galaxies was extracted from SDSS imaging. However, the u- and z-bands were excluded from our analysis in light of their low signal-to-noise (hereafter S/N) and the significant number of light profiles having obvious sky subtraction errors at those wavelengths (M11). The M11 NIR photometry came from a mixture of imaging sources, including the GOLDMine (Gavazzi et al. 2003, 78 galaxies) and Two Micron All-Sky Survey (Skrutskie et al. 2006, 20 galaxies) databases, while H-band imaging for the remaining (187) galaxies was obtained by M11 from April 2005 to May 2008 on Mauna Kea telescopes [ULBCAM (UH 2.2 m); WIRCAM (CFHT); WFCAM (UKIRT)]. The spatial extent of the NIR light profiles is, on average,  $\sim$ 60% that of the corresponding i-band profiles for  $\sim$ 200 galaxies (see §2.4 for our definition of profile extent), while the optical and NIR profiles reach median surface brightness levels of  $r \sim$  26.5 mag arcsec<sup>-2</sup> and  $H \sim$  23 mag arcsec<sup>-2</sup>, respectively. The high quality of the M11 light profiles enables a reliable investigation of Virgo galaxies' colours out to typically large galactocentric radii.

# 2.2. Surface brightness profiles and structural diagnostics

The *griH* major-axis surface brightness (hereafter SB) profiles of Virgo galaxies were extracted by M11 with the astronomical image-processing software XVISTA<sup>2</sup>. To ensure that colour gradients are computed homogeneously, the SDSS SB profiles were degraded to the (poorer) resolution of the NIR profiles.

We have also drawn upon the collection of non-parametric, H-band structural parameters presented in McDonald et al. (2009) to search for possible correlations between galaxy colour and structure. The structural parameters of interest include effective surface brightnesses ( $\mu_e$ ), effective radii ( $r_e$ ), concentrations ( $C_{28}$ ) and apparent magnitudes ( $m_H$ ). These non-parametric diagnostics all involve the extrapolation and integration of galaxies' NIR light profiles to infinity. We use the NIR values of the above structural diagnostics for their lower sensitivity to dust attenuation and greater sensitivity to the galaxy stellar masses.

# 2.3. Environmental diagnostics

To probe for an environmental dependence in the Virgo galaxy colours, we characterize the impact of environment with the neutral hydrogen deficiency parameter,  $Def_{HI}$ . For a cluster galaxy with a given gas mass  $M_{HI}$ ,  $Def_{HI} \equiv \langle \log M_{HI}(D_{opt,T}) \rangle$  -  $\log M_{HI}$ , where  $\langle \log M_{HI}(D_{opt,T}) \rangle$  is the typical HI mass for field galaxies of the same Hubble type, T, and optical diameter,  $D_{opt}$ , such that positive  $Def_{HI}$  values correspond to a dearth of neutral gas. The advantage of  $Def_{HI}$  as a measure of galaxy environment is its independence of projection effects that plague other traditional (2D) diagnostics (Solanes et al. 2002, hereafter S02). For completeness, we still appeal to the (projected) cluster-centric distances,  $D_{M87}$ , and local surface densities of the M11 galaxies,  $\Sigma$ , to assist our study of environmental effects on their colours. Cluster-centric distances were computed relative to M87 while assuming a common distance to all VCC galaxies of 16.5 Mpc (Mei et al. 2007). We follow Dressler (1980) in computing  $\Sigma$  as the number density comprised by the ten nearest VCC neighbours to a given galaxy's position.

We obtained  $Def_{HI}$  measurements for M11 galaxies from S02, Koopmann & Kenney (2004, hereafter KK04), and Gavazzi et al. (2005, hereafter G05). The latter compilation is the most complete, providing HI mass measurements for 91 of the 115 gas-rich galaxies in the M11 sample, as well as an additional 10 E/S0 systems. The other HI mass compilations have  $Def_{HI}$  determinations for 28 (KK04) and 53 (S02) galaxies, only four of which are not included in G05. We compare  $Def_{HI}$  measurements in Figure 1 for galaxies in common for KK04 and G02 with S02, with the

<sup>&</sup>lt;sup>2</sup>http://ganymede.nmsu.edu/holtz/xvista/

red line in each plot denoting equality. While there is good consistency between the KK04 and S02 databases (r = 0.97;  $\sigma = 0.11$  dex), the measurements of G05 are systematically higher on average than the others, regardless of morphology. Presuming that the G05 measurements are at least internally consistent, we rely strictly on that database for  $Def_{HI}$  values.

# 2.4. Surface brightness profile preparations

Prior to measuring Virgo galaxy colours and stellar populations, the M11 SB profiles require special attention, which we now describe. The computation of accurate galaxy colour profiles relies on accounting for pixels that are spoiled by either foreground stars, scattered light, or low S/N. To correct for this, we first truncated the M11 SB profiles by searching outward in each of them for a sequence of adjacent isophotes with SB errors in excess of a given threshold  $\sigma_{\mu,th}$ . The isophotes beyond that point were flagged as unreliable and their location marked as the truncation radius.

In the truncation process, we used error thresholds of 0.25 and 0.20 mag arcsec<sup>-2</sup> for the M11 optical and NIR SB profiles, respectively. These values correspond to locations in the SB profiles where the point-to-point scatter becomes comparable to the statistical errors per isophote. These thresholds are also roughly equal to 0.1-0.2% of the sky level (or less) in each profile.

We have also applied an adaptive radial binning scheme to the M11 SB profiles to increase the S/N per radial bin. While previous studies of galaxy colour gradients (e.g., MacArthur et al. 2004) used an incremental radial binning scheme, ours requires that a minimum signal-to-noise  $S/N_{\rm min}$  be met in all four bands in a given bin. Since an incremental scheme makes no such stipulation and typically has larger radial bins, the colour profiles of individual galaxies will then tend to extend further in this scheme than those determined from our adaptive scheme. However, these increased depths are overshadowed by the higher colour dispersions per radial bin and the inclusion of low S/N data points in galaxies' outskirts, thereby decreasing the quality of the colour profiles overall.

Accounting only for the Poisson noise of the source and sky, we calculate the S/N per isophote according to,

$$\frac{S}{N} = \frac{S_{\text{gal}}}{\sqrt{N_{\text{gal}}^2 + N_{\text{sky}}^2}}$$

$$= \frac{\mu_{\text{gal}} \times C_{\text{ell}}}{\sqrt{\mu_{\text{gal}} \times C_{\text{ell}} + \mu_{\text{sky}} \times C_{\text{ell}}}}$$

$$= \frac{\mu_{\text{gal}}}{\sqrt{\mu_{\text{gal}} + \mu_{\text{sky}}}} \times \sqrt{C_{\text{ell}}}, \tag{1}$$

where  $\mu_{\rm gal}$  and  $\mu_{\rm sky}$  are the isophote's SB and sky background, respectively, and  $C_{\rm ell}$  is its circumference.

The radial binning scheme for each galaxy is based on the SB profile with the lowest overall S/N; the latter usually corresponds to the g-band, followed by the H-band. We enforce a minimum bin size for each galaxy, which is set by the maximum seeing disk amongst all bands and most often corresponds to the H-band value. The SB of a bin is determined by a weighted average of the isophotal SBs that it contains, while the bin location is set to its midpoint. Through extensive testing, we have found that using the  $\sigma_{\mu}$ - $\mu$  median trends determined from the original photometry provided the most reliable way of estimating the SB error per bin. Lastly, we have carried out our analysis for the cases of  $S/N_{\min} = 10, 20, 30, 40$  and 50 per bin.

## 2.5. Sky errors

The determination of accurate colour gradients for a galaxy demands reliable subtraction of the sky's contribution to the flux measured within each filter. An under- or over-estimated sky in a given band will artificially increase or decrease the corresponding SB measured in a galaxy's outskirts, respectively, thereby skewing its colour profiles. Sky errors dominate all other error sources in the study of galaxy colours (Bell & de Jong 2000). While M11 took great care in assessing sky level corrections, our profile truncation algorithm (§2.4) is already effective before the sky error envelopes become prohibitively large (i.e.,  $\sigma_{\rm sky} \sim 0.2\%$  of the sky level). We revisit the issue of sky errors in §3.1.

#### 3. RESULTS & DISCUSSION

We now consider the broadband colour profiles of Virgo galaxies, as well as seek out possible morphological, structural and environmental trends in their central colours. These data offer a view of stellar populations both within and amongst galaxies, free of any assumptions about their underlying star formation histories and chemical evolution.

## 3.1. Colour profiles and gradients

The wide frequency baseline of the g-H colour provides us with our best constraint on the broad spectral shapes of Virgo galaxies, and thus on their stellar populations. The median g-H profiles and rms dispersions for Virgo galaxies of different morphologies are shown in Figure 2

by the solid and dashed lines, respectively. For this exercise, the g-H colour profile for each galaxy was created by subtracting its binned H-band light profile from its binned g-band light profile. We also scaled each colour profile according to the NIR effective radius of the galaxy, thereby removing the size variation that exists amongst galaxies of various Hubble types. Given our imposed S/N constraints, we find that the median colour profiles for the many Virgo galaxy types span a large range, extending out to  $\sim$ 6  $r_e$  for the gas-poor giants, down to  $\gtrsim$ 2  $r_e$  for the gas-rich dwarfs and irregulars.

As a complement to Figure 2, we list in Table 1 the relevant colour information for each morphological group (column 1). Columns 2-4 contain the median g-H colour gradients, where the gradient for each galaxy was measured from a linear fit to the g-H profile. The gradients were computed for three choices of radial coordinate, so that the median gradients could be expressed either in terms of scaled ( $r_e$ ; column 2) or physical radii (the latter were computed on both a linear and logarithmic scale; columns 3-4). Column 5 shows the median g-H central colours, while column 6 provides the number of galaxies in each morphological group. Both the central colours and colour gradients for each of our galaxies, along with their surface brightness profiles and bulge-disk decompositions, are available at the Centre de Données astronomiques de Strasbourg and our own website<sup>3</sup>.

In fitting galaxies' colour profiles, we neglected the first radial bin in order to avoid adverse PSF blurring effects from skewing our computed gradients. We show in Figure 3 the size of the first radial bin versus the FWHM of the maximum seeing disk for all Virgo galaxies. The proximity of many galaxies to the line of equality (red) indicates that seeing effects within the first bin of the colour profiles for those systems are likely non-negligible.

Other effects which could potentially skew the median colour gradient estimates provided in Table 1 include the use of a variable radial range in individual colour profile fits (given our choice of binning scheme) and of different  $S/N_{min}$  values in adaptively binning the M11 SB profiles. As shown in Figures 4 and 5 though, neither of these two effects presents a significant risk towards the robustness of our colour gradient determinations.

Examination of Table 1 reveals a large dispersion in the colour gradient distribution of each Virgo galaxy type. These dispersions may be either intrinsic to Virgo cluster galaxies, or largely the result of measurement errors in their SB profiles. As mentioned in §2.5, imperfect sky subtraction is the largest source of error in the computation of galaxy colour gradients. We can estimate the impact of sky errors on those gradients through the  $\pm 1\sigma_{sky}$  error envelopes for each M11 SB profile, where  $\sigma_{sky}$  is the standard deviation in the sky levels measured in boxes along the periphery of a given Virgo galaxy image. We assess the colour gradient error by calculating the extrema of this

<sup>&</sup>lt;sup>3</sup>www.astro.queensu.ca/virgo

quantity based on sky error envelopes. The distribution of errors in the g-H colour gradients of Virgo galaxies due to imperfect sky subtractions is shown in Figure 6. Comparing Figure 6 with Table 1, it can be seen that median sky errors contribute no more than  $\sim$ 16% of the dispersion found in the colour gradient distribution of each galaxy type; those dispersions are thus largely intrinsic to each galaxy population.

It is reassuring that the distribution of the median colour gradients listed in Table 1 accurately reflects our impressions from Figure 2, which we now describe<sup>4</sup>. Collectively, the median g-H profiles of Virgo galaxies exhibit intriguing features. First, most galaxy types (dE/dS0, Sa–Sd, Im, ?) are described by a negative colour gradient, albeit of differing strengths. The gas-poor E/S0's, Sdm+Sm spirals, star-forming BCDs, and morphologically-peculiar S? galaxy types, on the other hand, have either quasi-flat (E/S0, Sdm+Sm, BCD) or positive (S?) colour gradients. This variation in the g-H gradients of Virgo galaxies seems to correlate with morphology, such that the gradient is more negative for later Hubble types, as seen elsewhere (e.g., Jansen et al. 2000; La Barbera et al. 2002; Gonzalez-Perez et al. 2011). Although the large dispersions reported in Table 1 might draw suspicion on such a claim, comparisions of the gradient distributions for neighbouring morphologies via the Kolmogorov-Smirnov (KS) test confirms that the probability that any two distributions come from the same parent does not exceed  $\sim$ 40%.

On its own, our detected morphological trend in the median colour gradients of Virgo galaxies might seem surprising as previous studies of galaxy colours have failed to reveal the existence of such gradient (i.e., positive/negative) for most galaxy types (e.g., Kim & Ann 1990; Gadotti & dos Anjos 2001; Grant et al. 2005; Hunter & Elmegreen 2006; Liu et al. 2009). The dispersions in Table 1 show, however, that the colour gradient distribution for each Virgo galaxy type encompasses both positive and negative values, confirming that the variety in colour gradient sign found previously is reproduced here. Late-type spirals, on the other hand, have been shown by (Taylor et al. 2005) as having a robust (positive) colour gradient sign, which, interestingly enough, is contrary to the typically negative gradient that we find for Virgo Scd—Sm spirals. This discrepancy may be attributed to the fact that Taylor et al. used UV-optical colours, which are quite sensitive to the ongoing star formation that is likely occurring within these gas-rich galaxies.

Also interesting from Table 1 is the variation of the colour gradient dispersion amongst major galaxy types. For instance, the (rms) dispersion (in  $r_e$  space) for the Virgo gas-poor giants and spirals is  $\sim$ 0.21 and  $\sim$ 0.36, respectively. The irregulars have intermediate values. This result agrees with the significant scatter in both the colours and colour gradients of spiral galaxies that has been reported by many (Peletier & Balcells 1996; Taylor et al. 2005; Muñoz-Mateos et al. 2007;

<sup>&</sup>lt;sup>4</sup>The apparent contradictory behaviour exhibited in the outskirts of some median colour profiles (e.g., dE) is resolved by considering that the colour data in the outskirts have lower S/N than that which comprises the interiors

Ganda et al. 2009; West et al. 2009). The large colour ranges spanned by both Virgo spirals and irregulars may reflect a large variance in their stellar population properties due to their ongoing star formation. Dust attenuation may also be affecting these galaxies' colours, especially since the M11 sample contains a few unrealistically red  $(g-H \sim 4-5)$  Sa–Sd galaxies (see Figure 9). Whether the role of dust in setting galaxy colours is statistically important or not will be revisited in §3.2.4.

In addition to the collective properties and trends noted above, inspection of the median colour profiles amongst major Virgo galaxy types reveals other noteworthy results. For instance, within their respective errors, the profiles for the two gas-poor giant types (E/S0) are remarkably similar; both exhibit a relatively constant colour (g-H  $\sim$  3.2) out to  $\sim$ 4  $r_e$ , beyond which they become redder with radius. This suggests that Virgo E/S0's possess similar stellar populations and likely share a similar (extended) formation history; this idea is explored further in Paper II. On the other hand, Figure 2 and Table 1 remind us that Virgo gas-poor dwarfs are systematically bluer and have more negative colour gradients than the gas-poor giants. Indeed, KS tests of the colour gradient distributions for Virgo gas-poor dwarfs and giants only have a  $\sim$ 7% probability of having a common parent distribution. The colour gradients that we have found for Virgo gas-poor dwarfs are consistent with these galaxies being less enriched overall than Virgo gas-poor giants (Zaritsky et al. 1994; Tremonti et al. 2004; Paper II).

# 3.1.1. Comparison with literature

It is instructive to compare our optical-NIR colour gradient estimates with literature values for other galaxies. La Barbera et al. (2010) measured  $d(g-H)/d\log(r/r_e)$  colour gradients in 4546 giant gas-poor galaxies that overlap with both the SDSS and 2MASS to find a strongly negative mean value and large dispersion for them:  $-0.286 \pm 0.293$  mag/dex. The combined g-H colour gradient distribution for our Virgo E and S0 galaxies, equal to  $-0.245 \pm 0.426$  mag/dex, agrees well with La Barbera's result. Moreover, the analysis of the g-K colour gradient distribution for a smaller sample of nearby giant gas-poor galaxies by Wu et al. (2005) has also yielded a mean value similar to ours (-0.29 mag/dex).

With respect to gas-rich dwarf galaxies, Hunter & Elmegreen (2006) analysed the V-J colour gradients in both Magellanic irregulars and blue compact dwarfs and found that the mean colour gradient for these two galaxy types is -0.07 and +0.90 mag/kpc, respectively. While the mean g-H colour gradient that we have estimated for Virgo Im galaxy types (-0.11 mag/kpc) agrees well with the former, that for Virgo BCDs (+0.11 mag/kpc) is much flatter. This discrepancy is reduced when we consider the fact that the standard deviations about both mean values is large (1.129 and 0.318 mag/kpc, respectively) and that both distributions suffer from small sample sizes (N = 5 and 8, respectively).

Lastly, Muñoz-Mateos et al. (2007) studied the *FUV-K* colour gradients for spiral galaxies of all types. Although a quantitative comparison of FUV-*K* and *g-H* colours and colour gradients seems ill-conceived for any galaxy type, it is interesting to note that the median FUV-K colour gradient in these authors' sample decreases, albeit weakly, from early- to late-type spirals (-0.015 mag kpc<sup>-1</sup> for Sa–Sb's to -0.040 mag kpc<sup>-1</sup> for Scd+Sd's); their Sdm+Sm spirals do not follow this trend, however, having a nearly flat median gradient of -0.005 mag kpc<sup>-1</sup>. This morphological trend in the Muñoz-Mateos et al. data is similar to the one which we have found in terms of the *g-H* colour gradients of Virgo cluster spirals.

Based on these comparisons, encompassing a wide range of galaxy types, Virgo cluster galaxies exhibit radial colour distributions that are apparently similar to those of field and cluster galaxies found in other nearby galaxy catalogs.

## 3.2. Colour trends

# 3.2.1. Morphology

We now investigate trends in Virgo galaxy colours as a function of galaxy morphology, structure, environment and axis ratio. Beginning with morphology, we show colour-colour diagrams in Figures 7-9 for several galaxy types against the colour predictions from a stellar population model (black lines) in order to diagnose the effects of mean age  $\langle A \rangle$  (g-r; dashed) and metallicity Z (r-H; solid) in setting the Virgo galaxy colours. The model is an exponential star formation history with a variable timescale  $\tau$  and several fixed metallicities. Nominal values of both the  $\langle A \rangle$  and Z coordinates are indicated alongside the grid in each plot. Further details about this and other stellar population models are given in Paper II. The orange-red arrow represents the reddening vector for a dust screen, also discussed more fully in Paper II. Median values of both the calibration and sky errors in the M11 sample are shown in the lower-right corner of each plot, where the effect of the latter has been computed at both the centers and outskirts of Virgo galaxies. Note that both the model predictions and reddening vector discussed above have been included in Figures 10-12 as well.

Figures 7-9 show that the different Virgo galaxy types have unique colour profile combinations, and thus stellar contents. The colour profiles of the gas-poor systems (Figures 7-8) suggest that their stellar populations are old (>9 Gyr) and span a wide range in metallicity; that is, these colour gradients are largely explained as a metallicity effect (Vader et al. 1988; Franx et al. 1989; Tamura et al. 2000; Wu et al. 2005), while age variations make a secondary, but non-negligible, contribution (La Barbera et al. 2010; Suh et al. 2010; but see Bothun & Gregg 1990). The systematic differences in the median colour profiles between the Virgo gas-poor giants and dwarfs (§3.1)

are similarly explained by the stellar populations of the former being more metal-rich ( $\Delta \log Z \lesssim$  -0.25), but only slightly older ( $\sim$ 0.5 Gyr), than the latter. Interestingly, the dE's and E's together define the metallicity extrema for the entire Virgo gas-poor galaxy population, as opposed to the dS0's and S0's.

The Virgo irregulars (Figure 8) show the greatest colour range amongst all of the major galaxy types in this cluster such that, collectively, their stellar populations go from being old and metal-rich to young and metal-poor. This extreme colour variation extends to the Virgo irregulars as well, as their median colour profiles show that significant radial increases and decreases in age and metallicity, respectively, occur within each galaxy type. Such broad population gradients make it difficult to assign typical ages and metallicities to irregular galaxies. The offsetting effect that such radial behaviours in stellar populations have on colours helps explain previous reports of flat (or weakly positive) optical colour gradients in irregular galaxies (Kim & Ann 1990; Papaderos et al. 1996; Taylor et al. 2005). Moreover, the redder disks that have been found in dIrr's relative to those in BCDs (Patterson & Thuan 1996) may be understood by the former having older outskirts.

Age and metallicity gradients are also apparent within Virgo spirals (Figure 9), but with the latter being more significant, on average, than the former. Age and metallicity variations have been ascribed previously as the source of the significant colour gradients in spiral galaxies (de Jong 1996; Gadotti & dos Anjos 2001; La Barbera et al. 2003; MacArthur et al. 2004), while our claim that the implied age gradients in spirals are small is only matched by Peletier & Balcells (1996). In the median, the metallicity gradients for all Virgo spiral types appear to be uniformly negative, while their age gradients are more varied. This complex pattern of Virgo spirals' colour gradients thwarts any realistic estimate of typical ages and metallicities for these galaxies as well. However, the colours of Virgo spirals exhibit a morphological trend, also reported elsewhere (de Jong 1996; MacArthur et al. 2004), which may be explained by the earlier galaxies being older and more enriched than the later ones.

#### 3.2.2. Structure

We show in Figure 10 the same colour-colour diagram as in Figure 7 (including the same model) but with the points differentiated according to the following structural parameters:  $C_{28}$ ,  $m_H$ ,  $\mu_e$  or  $r_e$ . In these plots, we focus on galaxy centers (i.e., within an aperture of 0.5  $r_e$ ) to ease the distinction of colour trends as a function of galaxy structure. We also indicate with error bars the median values and rms dispersions of the colour distributions for all structural parameter bins.

The Virgo galaxy central colours exhibit multiple trends against structural parameters. The trend versus  $C_{28}$  suggests that the most concentrated Virgo galaxies are the oldest and most metal-

rich. Since  $C_{28}$  measures the shape/concentration of a galaxy's light profile, this trend essentially confirms that found above versus morphology between the Virgo spheroidal and disk galaxies. The other trends, with  $m_H$  and  $\mu_e$ , indicate that the more luminous and brighter Virgo galaxies tend to be older and more enriched than less luminous systems. Our detection of these trends agrees with the luminosity and surface brightness dependencies of galaxy colours and colour gradients reported in numerous studies (Vader et al. 1988; Peletier et al. 1990; Balcells & Peletier 1994; de Jong 1996; Jansen et al. 2000; Jerjen et al. 2000; Tamura & Ohta 2003; MacArthur et al. 2004; Liu et al. 2009) (but see Kim & Ann 1990 and La Barbera et al. 2004 for arguments against the luminosity dependence of gas-poor galaxies' colours). No significant colour trend is seen against  $r_e$  other than the most compact Virgo galaxies being older and more metal-rich than larger ones. This null result agrees with the weak size trends in spiral galaxies' colour gradients seen elsewhere (Muñoz-Mateos et al. 2007; Liu et al. 2009), though Parodi et al. (2002) reported a disk scale length dependence in the colour gradients of field and group dIrr's.

#### 3.2.3. Environment

Figure 11 is the environmental corollary to Figure 10. To investigate possible colour-environment trends, the M11 galaxies have been assigned in each of these figures to one of four equally-populated bins in the following parameters:  $D_{M87}$ ,  $\Sigma$ , or  $Def_{HI}$ . We find from these plots that the median colours of the different  $D_{M87}$  and  $\Sigma$  bins all roughly coincide, suggesting that cluster-centric location of, or local density about, a Virgo galaxy has little influence on its stellar content. This result is matched by Koo et al. (2005) and Muñoz-Mateos et al. (2007) who found no change in the colours or colour gradients of gas-rich galaxies with local density. The contradictory claim by (Parodi et al. 2002) about a density dependence of galaxy colours is diffused by considering that those authors used a sample which spanned a wider density baseline (field $\rightarrow$ cluster) than ours.

Amongst Virgo gas-rich galaxies, we find a clean trend of colours with  $Def_{HI}$ , such that more deficient systems are older and more metal-rich than less deficient ones. However, the comparable r-H colours found amongst intermediate- $Def_{HI}$  galaxies suggest that age effects dominate over those of metallicity in creating the observed trend. To our knowledge, this is the first report of a gas deficiency-colour correlation for Virgo galaxies. However, a latent correlation between the  $Def_{HI}$  measurements for our galaxies and their morphology, with a Pearson correlation coefficient of -0.68, makes it unclear whether the colour- $Def_{HI}$  trend is fundamental or not.

## 3.2.4. Dust

It would also be prudent to address the effects of dust on the colour properties of Virgo cluster galaxies. The presence of dust in star-forming systems is of concern in stellar population studies since reddened broadband colours may be erroneously attributed to their stellar content. For instance, the colour gradients of a galaxy with a smoothly-varying dust distribution may be taken as due to combined negative age and metallicity gradients within it, a consequence of the three-fold age-metallicity-dust degeneracy. Even face-on systems may be susceptible to such effects (Peletier et al. 1999, M04; Paper II). Moreover, Goudfrooij & de Jong (1995) have shown that the shallow optical colour gradients of gas-poor giants may be explained by a diffuse dust component, while Ganda et al. (2009) have found evidence for severe (but localized) dust attenuation in the optical-NIR profiles of nearby spirals.

In Figure 12, we assess the dust reddening of the central colours of Virgo spirals in the r-H versus g-r plane, where individual galaxies are identified according to their NIR axis ratio, b/a. In so doing, we find large dispersions in the colour distributions for edge-on systems, which suggests that some of them likely suffer from significant reddening. The colour centroids of the highest and lowest inclination spirals are nearly identical, however, which is inconsistent with dust being the main driver of these galaxies' central colours. That is, in a statistical sense, the effect of dust on our galaxy colours may be neglected. This conclusion finds ample support in the literature (de Jong 1996; Peletier & Balcells 1996; Gadotti & dos Anjos 2001; MacArthur et al. 2004), but does not preclude a possible contribution of dust to the colour gradients of individual systems (e.g., Peletier et al. 1995; La Barbera et al. 2003). Indeed, we find dramatic colour variations between adjacent radial bins in a few Virgo spirals, indicative of significant reddening at those (redward) locations (i.e., those colour variations would otherwise imply radical changes in local age and metallicity), but the incidence of such bins is small.

## 4. CONCLUSIONS

By combining high-quality optical (gri) and near-infrared (H) imaging for  $\sim 300$  Virgo cluster galaxies, we have studied the resolved broadband colours of a representative galaxy sample spanning the full range of structural parameters. Below is a summary of our main findings about Virgo galaxies' colour gradients and trends in their central colours with structural and environmental parameters:

• In the median, the colour gradients of Virgo galaxies systematically decrease with morphological type, such that the gradients of giant early-types are nearly flat, while those of later types are strongly negative (i.e., red centers to blue outskirts). The colour gradients of early-

type dwarfs are more negative than those for the giants;

- The colour gradients of all Virgo galaxies principally arise from stellar metallicity gradients, while stellar age gradients contribute only to the colours of Virgo irregulars;
- The central colours of Virgo galaxies correlate with concentration, luminosity, and surface brightness, such that galaxies become redder with an increase in each of these parameters;
- While the central colours of Virgo galaxies do not depend on cluster-centric distance or local galaxy density, those of Virgo gas-rich galaxies correlate strongly with their neutral gas deficiency;
- The central colours of Virgo spiral galaxies are uncorrelated with axial ratio, thus limiting the role of dust in setting their colours.

While the above results reflect on the stellar content of Virgo galaxies and their structural and environmental dependencies, we can explicitly apply stellar population models to galaxy colours. This is what we do in Paper II as a way to constrain formation scenarios for the major galaxy types in the Virgo cluster.

This research has made use of the NASA/IPAC extragalactic and GOLDMine databases. Funding for the SDSS has been provided by the Alfred P. Sloan Foundation, the Participating Institutions, the National Science Foundation, the US Department of Energy, the National Aeronautics and Space Administration, the Japanese Monbukagakusho, the Max Planck Society, and the Higher Education Funding Council for England. The SDSS Web Site is http://www.sdss.org/. The SDSS is managed by the Astrophysical Research Consortium for the Participating Institutions. The Participating Institutions are the American Museum of Natural History, Astrophysical Institute Potsdam, University of Basel, Cambridge University, Case Western Reserve University, University of Chicago, Drexel University, Fermilab, the Institute for Advanced Study, the Japan Participation Group, The Johns Hopkins University, the Joint Institute for Nuclear Astrophysics, the Kavli Institute for Particle Astrophysics and Cosmology, the Korean Scientist Group, the Chinese Academy of Sciences (LAMOST), Los Alamos National Laboratory, the Max-Planck-Institute for Astronomy, the Max-Planck-Institute for Astrophysics, New Mexico State University, The Ohio State University, University of Pittsburgh, University of Portsmouth, Princeton University, the United States Naval Observatory, and the University of Washington. J.R. and S.C. acknowledge financial support from the National Science and Engineering Council of Canada through a postgraduate scholarship and a Discovery Grant, respectively. We also thank Brent Tully for his help in the acquisition of H-band imaging of Virgo cluster galaxies (as reported in M11).

## **REFERENCES**

Abraham, R. G., Ellis, R. S., Fabian, A. C., Tanvir, N. R., & Glazebrook, K. 1999, MNRAS, 303, 641

Adelman-McCarthy, J. K., et al. 2007, ApJS, 172, 634

Adelman-McCarthy, J. K., et al. 2008, ApJS, 175, 297

Balcells, M., & Peletier, R. F. 1994, AJ, 107, 135

Barazza, F. D., Binggeli, B., & Prugniel, P. 2001, A&A, 373, 12

Barazza, F. D., Binggeli, B., & Jerjen, H. 2003, A&A, 407, 121

Bell, E. F., & de Jong, R. S. 2000, MNRAS, 312, 497

Bergvall, N., Rönnback, J., Masegosa, J., &Oumlstlin, G. 1999, A&A, 341, 697

Binggeli, B., Sandage, A., & Tammann, G. A. 1985, AJ, 90, 1681

Boselli, A., Boissier, S., Cortese, L., & Gavazzi, G. 2008, ApJ, 674, 742

Bothun, G. D., & Gregg, M. D. 1990, ApJ, 350, 73

Bremnes, T., Binggeli, B., & Prugniel, P. 1998, A&AS, 129, 313

Bremnes, T., Binggeli, B., & Prugniel, P. 1999, A&AS, 137, 337

Bremnes, T., Binggeli, B., & Prugniel, P. 2000, A&AS, 141, 211

Burstein, D., Faber, S. M., Gaskell, C. M., & Krumm, N. 1984, ApJ, 287, 586

Cardiel, N., Gorgas, J., Sánchez-Blázquez, P., Cenarro, A. J., Pedraz, S., Bruzual, G., & Klement, J. 2003, A&A, 409, 511

Courteau, S., de Jong, R. S., & Broeils, A. H. 1996, ApJ, 457, L73

de Jong, R. S. 1996, A&A, 313, 377

Dressler, A. 1980, ApJ, 236, 351

Faber, S. M. 1973, ApJ, 179, 731

Ferreras, I., Lisker, T., Carollo, C. M., Lilly, S. J., & Mobasher, B. 2005, ApJ, 635, 243

Ferreras, I., Lisker, T., Pasquali, A., & Kaviraj, S. 2009, MNRAS, 395, 554

Franx, M., Illingworth, G., & Heckman, T. 1989, AJ, 98, 538

Gadotti, D. A., & dos Anjos, S. 2001, AJ, 122, 1298

Gallagher, J. S., III, & Hunter, D. A. 1986, AJ, 92, 557

Gallazzi, A., Charlot, S., Brinchmann, J., White, S. D. M., & Tremonti, C. A. 2005, MNRAS, 362, 41

Ganda, K., Peletier, R. F., Balcells, M., & Falcón-Barroso, J. 2009, MNRAS, 395, 1669

Gavazzi, G., Bonfanti, C., Sanvito, G., Boselli, A., & Scodeggio, M. 2002, ApJ, 576, 135

Gavazzi, G., Boselli, A., Donati, A., Franzetti, P., & Scodeggio, M. 2003, A&A, 400, 451

Gavazzi, G., Boselli, A., van Driel, W., & O'Neil, K. 2005, A&A, 429, 439

Gil de Paz, A., & Madore, B. F. 2005, ApJS, 156, 345

Gonzalez-Perez, V., Castander, F. J., & Kauffmann, G. 2011, MNRAS, 411, 1151

Goudfrooij, P., Hansen, L., Jorgensen, H. E., Norgaard-Nielsen, H. U., de Jong, T., & van den Hoek, L. B. 1994, A&AS, 104, 179

Goudfrooij, P., & de Jong, T. 1995, A&A, 298, 784

Grant, N. I., Kuipers, J. A., & Phillipps, S. 2005, MNRAS, 363, 1019

Hunter, D. A., & Elmegreen, B. G. 2006, ApJS, 162, 49

James, P. A. 1994, MNRAS, 269, 176

James, P. A., Salaris, M., Davies, J. I., Phillipps, S., & Cassisi, S. 2006, MNRAS, 367, 339

Jansen, R. A., Franx, M., Fabricant, D., & Caldwell, N. 2000, ApJS, 126, 271

Jerjen, H., Binggeli, B., & Freeman, K. C. 2000, AJ, 119, 593

Kim, K. O., & Ann, H. B. 1990, Journal of Korean Astronomical Society, 23, 43

Ko, J., & Im, M. 2005, Journal of Korean Astronomical Society, 38, 149

Kobayashi, C., & Arimoto, N. 1999, ApJ, 527, 573

Koo, D. C., et al. 2005, ApJS, 157, 175

Koopmann, R. A., & Kenney, J. D. P. 2004, ApJ, 613, 866

La Barbera, F., Busarello, G., Merluzzi, P., Massarotti, M., & Capaccioli, M. 2002, ApJ, 571, 790

La Barbera, F., Busarello, G., Massarotti, M., Merluzzi, P., & Mercurio, A. 2003, A&A, 409, 21

La Barbera, F., Merluzzi, P., Busarello, G., Massarotti, M., & Mercurio, A. 2004, A&A, 425, 797

La Barbera, F., de Carvalho, R. R., Gal, R. R., Busarello, G., Merluzzi, P., Capaccioli, M., & Djorgovski, S. G. 2005, ApJ, 626, L19

La Barbera, F., & de Carvalho, R. R. 2009, ApJ, 699, L76

La Barbera, F., de Carvalho, R. R., de la Rosa, I. G., Gal, R. R., Swindle, R., & Lopes, P. A. A. 2010, arXiv:1006.4056

Liu, C.-Z., Shen, S.-Y., Shao, Z.-Y., Chang, R.-X., Hou, J.-L., Yin, J., & Yang, D.-W. 2009, Research in Astronomy and Astrophysics, 9, 1119

MacArthur, L. A., Courteau, S., Bell, E., & Holtzman, J. A. 2004, ApJS, 152, 175

MacArthur, L. A. 2005, ApJ, 623, 795

MacArthur, L. A., González, J. J., & Courteau, S. 2009, MNRAS, 395, 28

McDonald, M., Courteau, S., & Tully, R. B. 2009, MNRAS, 394, 2022

McDonald, M., Courteau, S., Tully, R. B., & Roediger, J. C. 2011, MNRAS, in press

McLaughlin, D. E. 1999, ApJ, 512, L9

Mei, S., et al. 2007, ApJ, 655, 144

Menanteau, F., et al. 2004, ApJ, 612, 202

Michard, R. 1999, A&AS, 137, 245

Michard, R. 2000, A&A, 360, 85

Moriondo, G., et al. 2001, A&A, 370, 881

Moth, P., & Elston, R. J. 2002, AJ, 124, 1886

Muñoz-Mateos, J. C., Gil de Paz, A., Boissier, S., Zamorano, J., Jarrett, T., Gallego, J., & Madore, B. F. 2007, ApJ, 658, 1006

Papaderos, P., Loose, H.-H., Thuan, T. X., & Fricke, K. J. 1996, A&AS, 120, 207

Parodi, B. R., Barazza, F. D., & Binggeli, B. 2002, A&A, 388, 29

Patterson, R. J., & Thuan, T. X. 1996, ApJS, 107, 103

Peletier, R. F., & Valentijn, E. A. 1989, Ap&SS, 156, 127

Peletier, R. F., Davies, R. L., Illingworth, G. D., Davis, L. E., & Cawson, M. 1990, AJ, 100, 1091

Peletier, R. F., Valentijn, E. A., Moorwood, A. F. M., Freudling, W., Knapen, J. H., & Beckman, J. E. 1995, A&A, 300, L1

Peletier, R. F., & Balcells, M. 1996, AJ, 111, 2238

Peletier, R. F., Balcells, M., Davies, R. L., Andredakis, Y., Vazdekis, A., Burkert, A., & Prada, F. 1999, MNRAS, 310, 703

Peletier, R. F., et al. 2007, MNRAS, 379, 445

Pierini, D. 2002, MNRAS, 330, 997

Searle, L., Sargent, W. L. W., & Bagnuolo, W. G. 1973, ApJ, 179, 427

Silva, D. R., & Elston, R. 1994, ApJ, 428, 511

Skrutskie, M. F., et al. 2006, AJ, 131, 1163

Solanes, J. M., Sanchis, T., Salvador-Solé, E., Giovanelli, R., & Haynes, M. P. 2002, AJ, 124, 2440

Suh, H., Jeong, H., Oh, K., Yi, S. K., Ferreras, I., & Schawinski, K. 2010, ApJS, 187, 374

Tamura, N., & Ohta, K. 2000, AJ, 120, 533

Tamura, N., Kobayashi, C., Arimoto, N., Kodama, T., & Ohta, K. 2000, AJ, 119, 2134

Tamura, N., & Ohta, K. 2003, AJ, 126, 596

Taylor, V. A., Jansen, R. A., Windhorst, R. A., Odewahn, S. C., & Hibbard, J. E. 2005, ApJ, 630, 784

Terlevich, R., Davies, R. L., Faber, S. M., & Burstein, D. 1981, MNRAS, 196, 381

Terndrup, D. M., Davies, R. L., Frogel, J. A., Depoy, D. L., & Wells, L. A. 1994, ApJ, 432, 518

Tinsley, B. M., & Gunn, J. E. 1976, ApJ, 203, 52

Tortora, C., Napolitano, N. R., Cardone, V. F., Capaccioli, M., Jetzer, P., & Molinaro, R. 2010, MNRAS, 407, 144

Trager, S. C., Faber, S. M., Worthey, G., & González, J. J. 2000, AJ, 119, 1645

Tremonti, C. A., et al. 2004, ApJ, 613, 898

Tamm, A., & Tenjes, P. 2006, A&A, 449, 67

Tully, R. B., Verheijen, M. A. W., Pierce, M. J., Huang, J.-S., & Wainscoat, R. J. 1996, AJ, 112, 2471

Vader, J. P., Vigroux, L., Lachieze-Rey, M., & Souviron, J. 1988, A&A, 203, 217

van Zee, L., Barton, E. J., & Skillman, E. D. 2004, AJ, 128, 2797

West, A. A., Garcia-Appadoo, D. A., Dalcanton, J. J., Disney, M. J., Rockosi, C. M., & Ivezić, Ž. 2009, AJ, 138, 796

Worthey, G., Faber, S. M., & Gonzalez, J. J. 1992, ApJ, 398, 69

Worthey, G. 1994, ApJS, 95, 107

Wu, H., Shao, Z., Mo, H. J., Xia, X., & Deng, Z. 2005, ApJ, 622, 244

Zaritsky, D., Kennicutt, R. C., Jr., & Huchra, J. P. 1994, ApJ, 420, 87

This preprint was prepared with the AAS LATEX macros v5.2.

Table 1. Median g-H colours and colour gradients of Virgo galaxies

Morphology		$\frac{d(g-H)}{dr}^{a}$		(g-H) <sub>0</sub>	N
(1)	$r/r_e \text{ (mag } r_e^{-1}\text{)}$ (2)	$r (\text{mag kpc}^{-1})$ (3)	$\log r (\text{mag dex}^{-1})$ (4)	(5)	(6)
dS0	$-0.126 \pm 0.199$	$-0.080 \pm 0.165$	$-0.198 \pm 0.290$	$3.000 \pm 0.220$	19
dE	$-0.177 \pm 0.208$	$-0.167 \pm 0.196$	$-0.309 \pm 0.377$	$2.843 \pm 0.184$	51
E	$-0.084 \pm 0.199$	$-0.075 \pm 0.339$	$-0.267 \pm 0.572$	$3.253 \pm 0.353$	32
S0	$-0.046 \pm 0.212$	$-0.028 \pm 0.152$	$-0.115 \pm 0.310$	$3.283 \pm 0.280$	53
Sa–Sb	$-0.138 \pm 0.314$	$-0.057 \pm 0.080$	$-0.322 \pm 0.424$	$3.274 \pm 0.578$	24
Sbc+Sc	$-0.190 \pm 0.324$	$-0.066 \pm 0.101$	$-0.428 \pm 0.407$	$3.176 \pm 0.663$	15
Scd+Sd	$-0.259 \pm 0.412$	$-0.106 \pm 0.180$	$-0.371 \pm 0.652$	$3.037 \pm 0.588$	17
Sdm+Sm	$-0.017 \pm 0.467$	$-0.009 \pm 0.231$	$-0.072 \pm 0.616$	$2.459 \pm 0.420$	9
Im	$-0.181 \pm 0.391$	$-0.076 \pm 0.278$	$-0.228 \pm 0.662$	$2.302 \pm 0.499$	13
BCD	$+0.051 \pm 0.233$	$+0.071 \pm 0.321$	$+0.197 \pm 0.403$	$2.355 \pm 0.417$	8
S?	$+0.141 \pm 0.400$	$+0.108 \pm 0.213$	$+0.158 \pm 0.468$	$2.415 \pm 0.466$	9
?	$-0.137 \pm 0.178$	$-0.077 \pm 0.266$	$-0.246 \pm 0.479$	$2.850 \pm 0.422$	8

<sup>&</sup>lt;sup>a</sup>The median colour gradients for Virgo galaxies were computed for three choices of radial coordinate: effective radii (*left*), kiloparsec (*center*), and logarithmic (*right*).

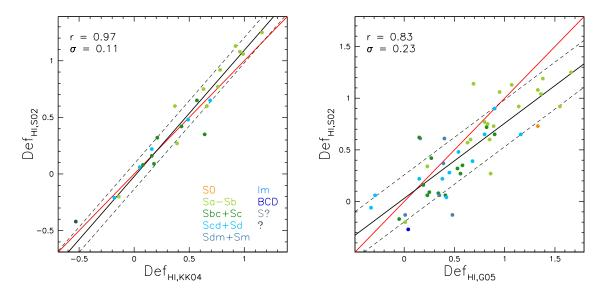


Fig. 1.— (*left*) Comparison of  $Def_{HI}$  measurements for Virgo galaxies in common between S02 and KK04. The red line has slope unity, while the solid and dashed black lines represent a linear fit to the data and the  $1\sigma$  deviation about the fit, respectively. The Pearson (linear) correlation coefficient r and  $\sigma$  of the fit are both provided in the top-left corner. (*right*) Same as left, but comparing S02 and G05.

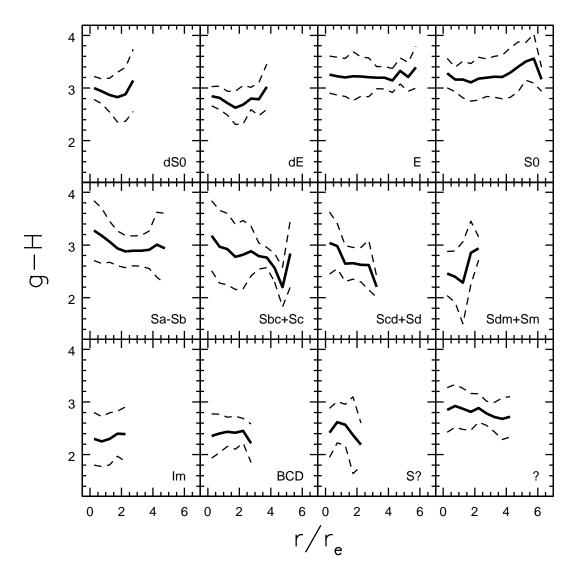


Fig. 2.— g-H profiles as a function of scaled radius,  $r/r_e$ , for Virgo galaxies binned by morphological type. The median profiles and their  $1\sigma$ -dispersion are indicated by the solid and dashed lines, respectively.

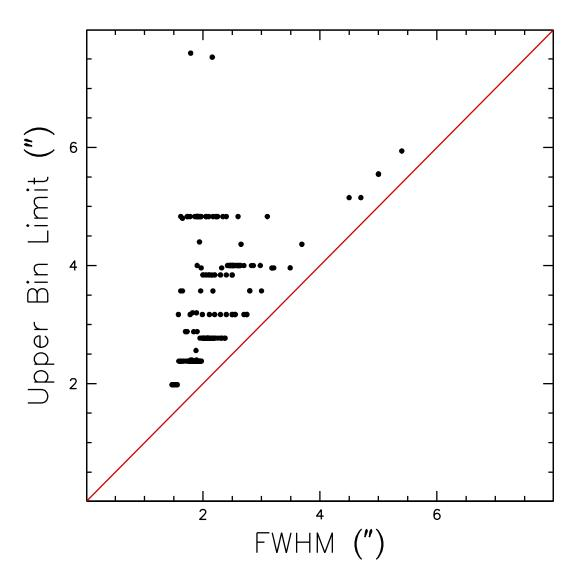


Fig. 3.— Size of the first radial bin versus the FWHM of the maximum seeing disk for Virgo galaxies. The 1:1 relation is marked by the red line.

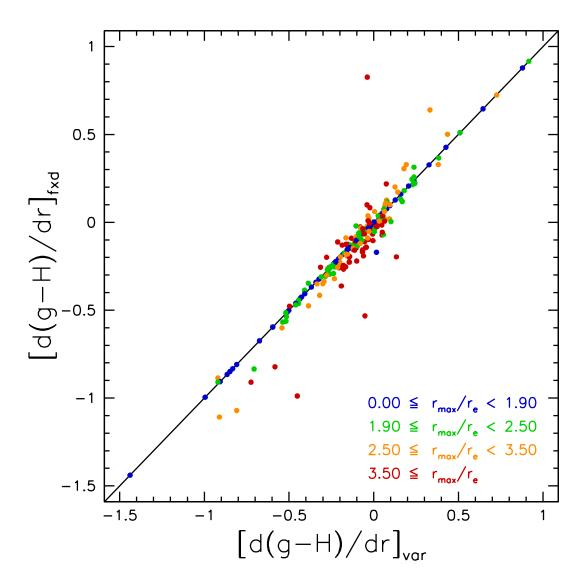


Fig. 4.— Comparison of the g-H colour gradients for Virgo galaxies determined using either a fixed or variable radial range in the linear fits to the colour profiles of individual galaxies. The data point colours reflect the maximum extent of each galaxy colour profile. For the fixed radial range fits, only data points within  $r < 2r_e$  were included. The black line marks the 1:1 relation.

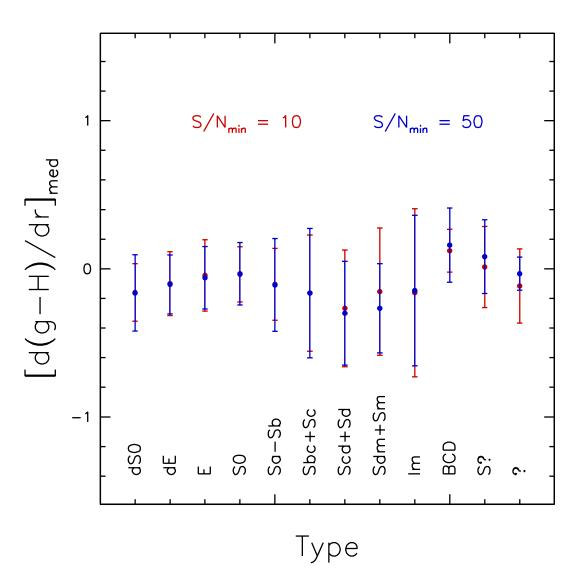


Fig. 5.— Comparison of the median g-H colour gradient estimates (as determined in  $r_e$  space) for Virgo galaxies, binned by morphological type, using a minimum S/N of either 10 or 50. The size of the error bars reflects the  $1\sigma$  (rms) dispersion within each morphological bin.

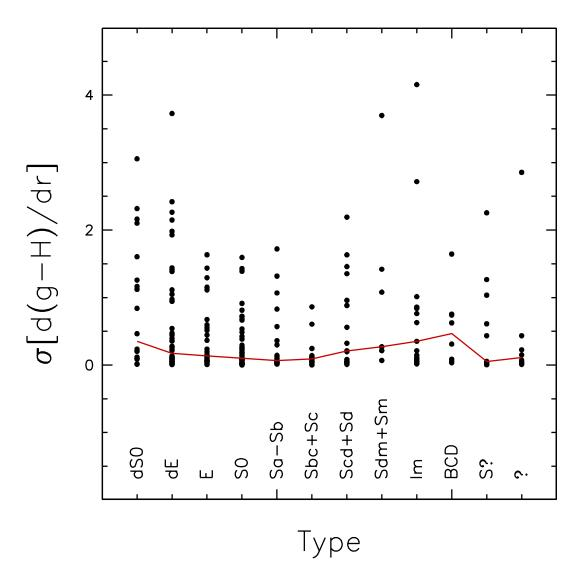


Fig. 6.— The (potential) contribution of sky subtraction errors to the estimated colour gradients (in  $r_e$  space) of individual Virgo galaxies, binned by morphological type. The red line connects the median error within each morphological bin.

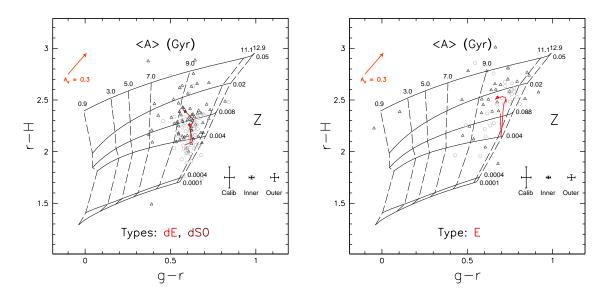


Fig. 7.— (*left*) r-H versus g-r colour-colour diagrams for Virgo dE and dS0 systems. Stars and filled circles represent the radial bins which enclose the galaxy centers and effective radii, respectively, while the coloured lines show the median colour profiles for both galaxy types. The grid represents a stellar population model for an exponential star formation history with no chemical evolution. The dashed and solid black lines correspond to lines of constant mean age and metallicity, respectively, with representative values indicated throughout the grid. The metallicities are expressed in percentages, according to mass contribution (i.e.,  $Z_{\odot} = 0.02$ ). The error bars shown at lower-right indicate the typical uncertainties in the measured colours due to both calibration and sky subtraction errors for the entire sample (the latter is shown for both galaxies' central and outermost radial bins). The orange-red arrow in the top-left corner shows the reddening vector of a foreground dust screen model for the indicated amount of extinction. (right) Same as left but for Virgo E galaxies.

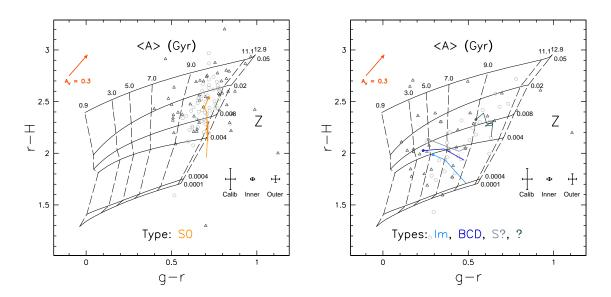


Fig. 8.— Same as Fig. 7 for Virgo lenticular (*left*) and irregular (*right*) galaxies.

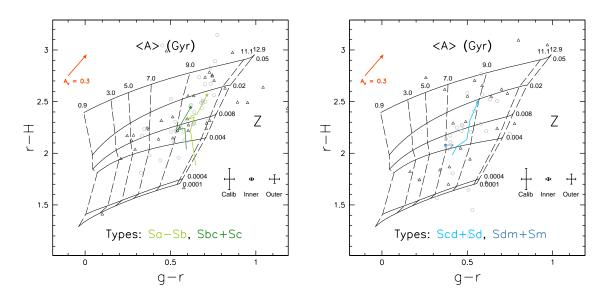


Fig. 9.— Same as Fig. 7 for Virgo spiral galaxies of types Sa–Sc (left) and Scd–Sm (right).

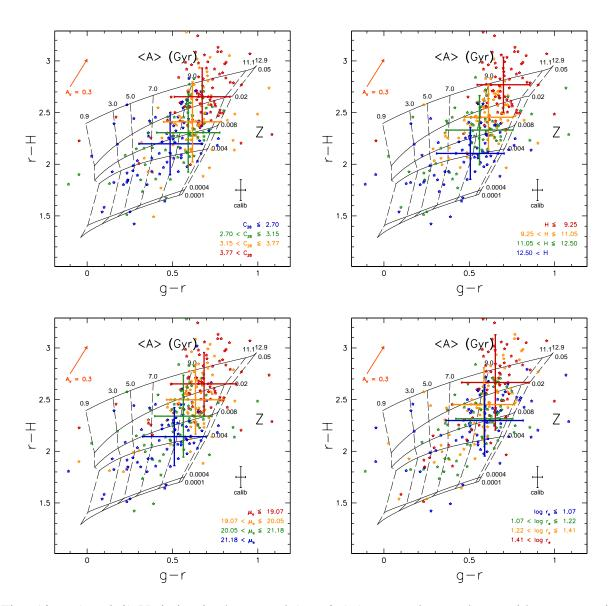


Fig. 10.— (top left) Variation in the central  $(r < 0.5r_e)$  r-H and g-r colours with concentration  $C_{28}$  for Virgo galaxies. Galaxies have been grouped into equally-populated bins by  $C_{28}$ , with the bin ranges and point colours indicated in the lower-right corner of the window. The overplotted error bars show both the centroid and rms scatter of the colour distribution within each  $C_{28}$  bin. The other plots are the same as at top-left, but show the variations in central r-H and g-r colours of Virgo galaxies with apparent magnitude  $m_H$  (top right), effective surface brightness  $\mu_e$  (bottom left), and effective radius  $r_e$  (bottom right).

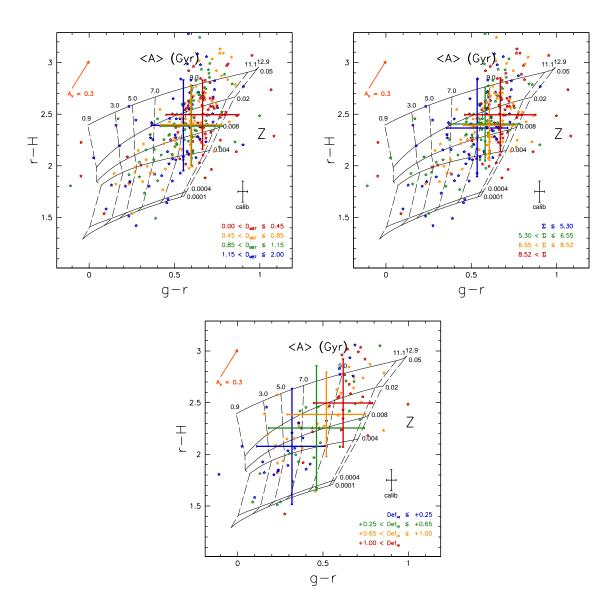


Fig. 11.— Same as Fig. 10 but showing variations in central r-H and g-r colours of Virgo galaxies with distance from M87  $D_{M87}$  (top left), local galaxian surface density  $\Sigma$  (top right) and neutral gas deficiency  $Def_{HI}$  (bottom). The plot against  $Def_{HI}$  only includes 101 galaxies due to the limited HI mapping of the Virgo cluster.

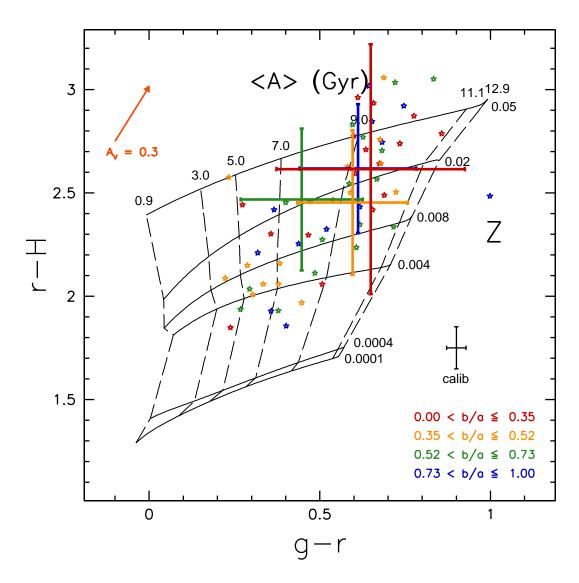


Fig. 12.— Same as Fig. 10 but showing variations in central r-H and g-r colours of Virgo galaxies with H-band axis ratio, b/a. Only the colours of Virgo spiral galaxies are plotted here.